Journal of Materials Chemistry

Cite this: J. Mater. Chem., 2012, 22, 21412

www.rsc.org/materials

PAPER

Phase evolution, phase transition, and microwave dielectric properties of scheelite structured $xBi(Fe_{1/3}Mo_{2/3})O_4$–$(1-x)BiVO_4$ ($0.0 \leq x \leq 1.0$) low temperature firing ceramics

Di Zhou,*[a] Li-Xia Pang,[b] Jing Guo,[a] Ze-Ming Qi,[c] Tao Shao,[c] Xi Yao[a] and Clive A. Randall[d]

Received 13th July 2012, Accepted 21st August 2012
DOI: 10.1039/c2jm34603f

In the present work, the $xBi(Fe_{1/3}Mo_{2/3})O_4$–$(1-x)BiVO_4$ ($0.0 \leq x \leq 1.0$) ceramics were prepared *via* the solid state reaction method. All the ceramics can be densified at low sintering temperatures around 820 °C. At room temperature, the $BiVO_4$ type scheelite monoclinic solid solution was formed in ceramic samples with a composition of $x \leq 0.10$. When x lies between 0.1 and 0.7, a $BiVO_4$ scheelite tetragonal phase is formed at room temperature. In the range $0.7 \leq x < 0.9$, the ceramic samples were found to be composites consisting of $BiVO_4$ type tetragonal and $Bi(Fe_{1/3}Mo_{2/3})O_4$ type monoclinic scheelite phases, and when $x \geq 0.9$, the $Bi(Fe_{1/3}Mo_{2/3})O_4$ type monoclinic scheelite solid solution was formed. In the $BiVO_4$ type monoclinic solid solution region, the phase transition to tetragonal phase was studied by *in situ* Raman and Far-Infrared spectroscopies and by thermal expansion analysis. All of these methods indicated that the phase transition temperature almost linearly decreased from 255 °C for pure $BiVO_4$ to about −9 °C for $x = 0.1$ sample. High performance microwave dielectric properties with a high permittivity of about 74.8, high Qf values above 11 500 GHz, and a small temperature coefficient of resonant frequency within +20 ppm per °C in a wide temperature range of 20–140 °C can be obtained in the composite ceramic sample with 60 mol% $x = 0.10$ composition and 40 mol% $x = 0.02$ composition. The $xBi(Fe_{1/3}Mo_{2/3})O_4$–$(1-x)BiVO_4$ ($0.0 \leq x \leq 1.0$) ceramics might provide useful candidate materials for microwave integrated capacitive devices, such as filters, antennas, *etc.*

I. Introduction

The general compositional formula for oxides with a scheelite structure is ABO_4, where the B cation is tetrahedrally coordinated to oxygen and the A cation is coordinated to eight oxygens from eight different tetrahedra. As indicated in Sleight and Linn's classic work,[1] the oxidation states range from one to four for the A site cations and from four to seven for the B site cations. Large concentrations of metal vacancies can be soluble on the A site, and the anion can be partially substituted with nitrogen and/or fluorine. The flexibility in substitutional chemistry and stoichiometry in the scheelite structure leads to great freedom in the structure and properties and permits diverse applications of catalytic properties, electric properties, and dielectric properties. As an example, the monoclinic scheelite $BiVO_4$ material has attracted attention due to its ferroelastic properties, dielectric properties at high frequency, high ion conductors, and photocatalytic properties.[1–6]

The $Bi(Fe_{1/3}Mo_{2/3})O_4$ ($Bi_3FeMo_2O_{12}$) phase was first synthesized by Sleight and Jeitschko[7] in 1974. Then a detailed characterization of this phase was studied,[8] and its importance grew due to its novel catalytic properties.[9] These materials were also of interest from a crystal chemical perspective, as it was found that $Bi_3FeMo_2O_{12}$ represented the first example of a trivalent cation on the tetrahedral sites of the $CaWO_4$ type scheelite structure, in which the FeO_4 and MoO_4 tetrahedra can take an ordered arrangement. In our previous work,[10] it was found that the $Bi_3FeMo_2O_{12}$ ceramic can be densified at around 830 °C and possessed microwave dielectric properties with a permittivity of ~27.2, a Qf value of ~14 500 GHz, and a temperature coefficient of −80 ppm per °C, which opens up this material as a new candidate dielectric for low temperature co-fired ceramics technology (LTCC).

Recently, a number of novel phase transitions, solid solutions, band gap information, and high performance microwave dielectric properties have been characterized in the (Li,Bi)(Mo,V)O_4, (Na,Bi)(Mo,V)O_4, and (K,Bi)(Mo,V)O_4 systems.[11–14] Besides low sintering temperatures between 650 and 830 °C, these

[a]*Electronic Materials Research Laboratory, Key Laboratory of the Ministry of Education & International Center for Dielectric Research, Xi'an Jiaotong University, Xi'an 710049, Shaanxi, China. E-mail: zhoudi1220@gmail.com; Fax: +86-29-82668794; Tel: +86-29-82668679*
[b]*Micro-optoelectronic Systems Laboratories, Xi'an Technological University, Xi'an 710032, Shaanxi, China*
[c]*National Synchrotron Radiation Laboratory, University of Science and Technology of China, Hefei, Anhui, 230029, China*
[d]*The Pennsylvania State University, Center for Dielectric Studies, Materials Research Institute, University Park, PA 16802, USA*

materials also have microwave dielectric properties, with permittivities between 75 and 81, Qf values between 8000 GHz and 10 000 GHz, and small band gap energy values of about 2.1 eV at room temperature in the compositions near the phase boundary between tetragonal and monoclinic scheelite phases. In the present work, the phase evolution, phase transition, microwave dielectric properties, and their relationships for the scheelite structured xBi($Fe_{1/3}Mo_{2/3}$)O_4–(1−x)$BiVO_4$ ($0.0 \leq x \leq 1.0$) were studied.

II. Experimental

Proportionate amounts of reagent-grade starting materials of Bi_2O_3 (>99%, Shu-Du Powders Co. Ltd., Chengdu, China), Fe_2O_3, V_2O_5 (>99%, Sinopharm Chemical Reagent Co., Ltd, Shanghai, China), and MoO_3 (>99%, Fuchen Chemical Reagents, Tianjin, China) were measured according to the stoichiometric formulation xBi($Fe_{1/3}Mo_{2/3}$)O_4–(1−x)$BiVO_4$ ($0.0 \leq x \leq 1.0$) (abbreviated here as BFMBVx). Powders were mixed and milled for 4 h using a planetary mill (Nanjing Machine Factory, Nanjing, China) by setting the running speed at 150 rpm with the zirconia balls (2 mm in diameter) as milling media. The powder mixture was then dried and calcined at 700 °C for 4 h. The calcined powders were ball milled for 5 h, with a running speed of 200 rpm to obtain fine powders. Then the powders were re-calcined at 700 °C and re-milled for better homogeneity. Then powders were pressed into cylinders (10 mm diameter and 4–5 mm height) in a steel die with 5 wt% PVA binder addition under a uniaxial pressure of 200 MPa. The composite samples were pressed into cylinders with different granulated powders (sieved through a mesh screen of 250 μm openings) of BFMBV0.02 and BFMBV0.10 samples. Samples were sintered in the temperature range from 780 °C to 840 °C for 2 h. Room temperature XRD was performed using XRD with Cu Ka radiation (the wavelength of $K\alpha_1$ and $K\alpha_2$ is 0.15406 nm and 0.5443 nm, respectively) (Rigaku D/MAX-2400 X-ray diffractometry, Tokyo, Japan). Prior to examination, sintered pellets were crushed in a mortar and pestle to powder. Diffraction pattern was obtained between 15 and 65° 2θ at a step size of 0.02°. To examine the grain morphology, as-fired surfaces were examined by scanning electron microscopy (SEM) (JSM-6460, JEOL, Tokyo, Japan). The Raman spectra at room temperature were obtained on polished pellets with a Raman spectrometer (inVia, Renishaw, England), excited by an Ar^+ laser (514.5 nm). The high temperature Raman spectra were measured using another Raman spectrometer (Lab-RAM HR800, HORIBA Jobin Yvon, France). The room temperature and *in situ* infrared reflectivity spectra were measured using a Bruker IFS 66v FTIR spectrometer on the infrared beamline station (U4) at National Synchrotron Radiation Lab. (NSRL), China. Dielectric properties at microwave frequency were measured by the $TE_{01\delta}$ dielectric resonator method with a network analyzer (HP 8720 Network Analyzer, Hewlett-Packard) and a temperature chamber (Delta 9023, Delta Design, Poway, CA). The temperature coefficient of resonant frequency TCF (τ_f) was calculated with the following formula:

$$\mathrm{TCF}(\tau_f) = \frac{f_T - f_{T_0}}{f_{T_0} \times (T - T_0)} \times 10^6 \quad (1)$$

where f_T and f_{T_0} were the $TE_{01\delta}$ resonant frequencies at temperature T and T_0, respectively.

III. Results and discussions

Phase evolution analysis by XRD and Raman

The room temperature X-ray diffraction data for xBi($Fe_{1/3}Mo_{2/3}$)O_4–(1−x)$BiVO_4$ ($0.0 \leq x \leq 1.0$) ceramics sintered at 800 °C are shown in Fig. 1(a) and (b). As the x value increased from 0.0 to 0.10, the crystal structure continuously changed from monoclinic to tetragonal along with the merging of the characteristic diffraction peaks, such as (1 0 1) and (0 1 1), (2 0 0) and (0 2 0), (2 0 4) and (0 2 4), *etc.* This result is similar to that in the ($A_{0.5x}Bi_{1-0.5x}$)(Mo_xV_{1-x})O_4 (A = Li, Na and K) systems, and the monoclinic scheelite solid solubility limit is typically around 10%.[11–14] In the B-site of the ABO_4 scheelite structure, the 4-coordinated Fe^{3+}, V^{5+} and Mo^{6+} cations have radii of 0.49 Å, 0.355 Å, and 0.41 Å, respectively, while 8-coordinated Bi^{3+}, Li^+, Na^+, K^+ atoms have radii of 1.17 Å, 0.92 Å, 1.18 Å, 1.51 Å, respectively, on the A-site, according to Shannon's data.[15] From our results and earlier studies, it can be deduced that 10% substitution for V ion on the B site by ions with bigger radii can destroy the monoclinic structure independent of the substitution for the A site with larger or smaller ions. The characteristic crystal structure difference between the scheelite monoclinic and tetragonal structures is that in the monoclinic phase, the B–O_4 tetrahedra have two O anions at the top, further apart than those at the bottom, which are located in one tetrahedral and give one long B–O distance and a shorter one ($B–O_1 > B–O_2$). However, the two different bond lengths $B–O_1$ and $B–O_2$ are equal to each other in the tetragonal phase. Hence, it is understandable that the equivalent ionic radius on the B site determines the bond length of BO_4 and consequently controls the phase transition in the ABO_4 scheelite structure. As seen in Fig. 1(b), a Bi($Fe_{1/3}Mo_{2/3}$)O_4 structured solid solution can be formed in the range $0.90 \leq x \leq 1.0$. In the range $0.70 \leq x \leq 0.85$, a composite region with both Bi($Fe_{1/3}Mo_{2/3}$)O_4 structured monoclinic and scheelite tetragonal solid solutions can be revealed. Due to the overlapping of the main peaks of the tetragonal and the Bi($Fe_{1/3}Mo_{2/3}$)O_4 monoclinic phases at around 28.5°, the composite phases region can be derived from the intensity differences for (3 1 0) and ($\bar{1}$ 1 1) peaks, (2 2 1) and ($\bar{4}$ 2 1) peaks, (6 0 0) and ($\bar{2}$ 0 2) peaks, *etc.* The cell parameters a and b and the phase composition as a function of x value are plotted in Fig. 1(c). It can be seen that as the x value increased from 0 to 0.10, the cell parameter a decreased, while b increased and became equal with each other at $x = 0.10$. With a further increase of x value to about 0.70, the cell parameter a increased to about 5.25 Å and remained stable in the composite phase region of $0.70 \leq x \leq 0.90$. There is no remarkable change in the cell parameters of Bi($Fe_{1/3}Mo_{2/3}$)O_4 monoclinic solid solution (a was divided by 3 to compare with that of the tetragonal phase). To better understand the relationship between the Bi($Fe_{1/3}Mo_{2/3}$)O_4 monoclinic and scheelite tetragonal structures, the schematic crystal structures are shown in Fig. 1(d)–(f). The crystal structure of Bi($Fe_{1/3}Mo_{2/3}$)O_4 can be simply understood as three times enlarged along *ab*-plane compared with the normal scheelite structure, and the ordered FeO_4 and MoO_4 tetrahedra arrangement can be clearly observed along the *a*-axis.

The room temperature Raman spectra of xBi($Fe_{1/3}Mo_{2/3}$)O_4–(1−x)$BiVO_4$ ($0.0 \leq x \leq 1.0$) ceramics are shown in Fig. 2(a). The typical Raman modes for pure $BiVO_4$ are marked and the

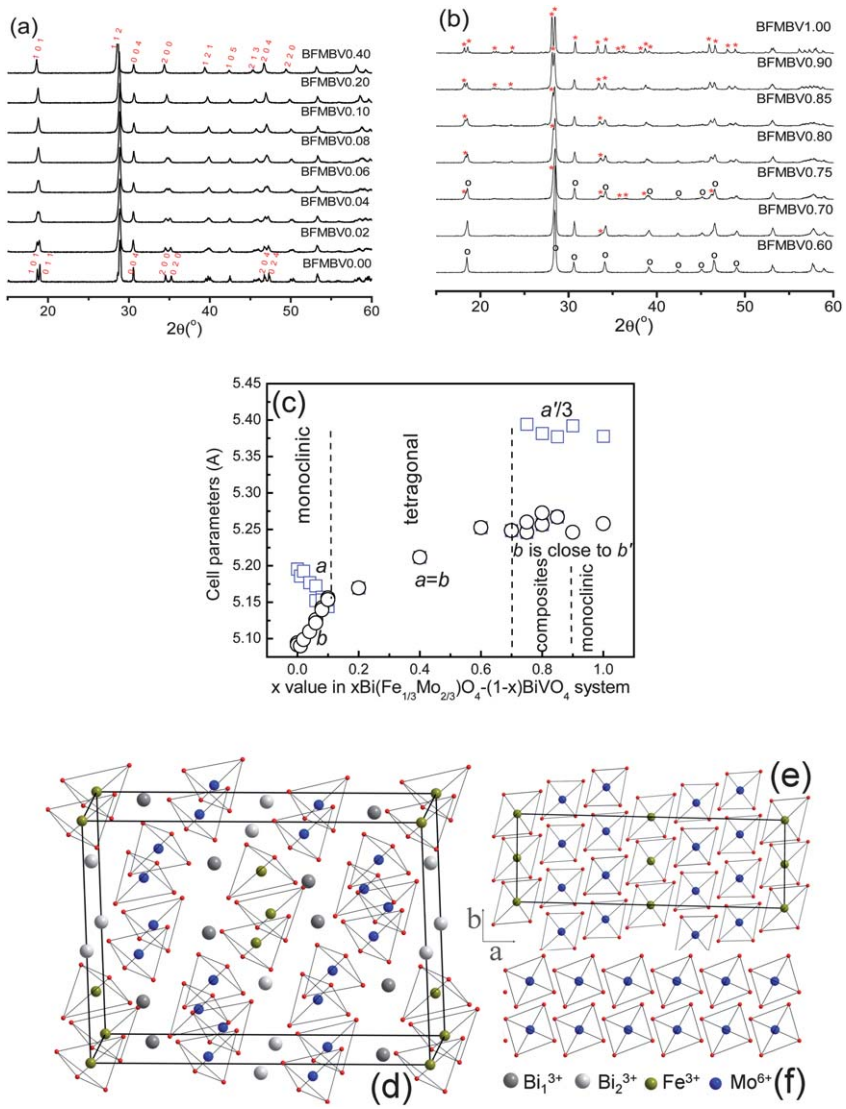

Fig. 1 X-ray diffraction data for xBi(Fe$_{1/3}$Mo$_{2/3}$)O$_4$–(1−x)BiVO$_4$ ($0.0 \leq x \leq 1.0$) ceramics sintered at 800 °C (a and b); cell parameters a and c as a function of x value (c); the schematic illustrations of the crystal structure of Bi(Fe$_{1/3}$Mo$_{2/3}$)O$_4$ (d); the network comparison along the ab-plane between ordered (e) and normal (f) scheelite structures.

detailed assignments can be found in our previous work.[11,12] As the x value increased from 0 to 0.10, the characteristic change is the merging of the δ_s(VO$_4$) (B_g) and δ_{as}(VO$_4$) (A_g) modes at around 366.8 and 325.3 cm^{-1}, respectively, for pure BiVO$_4$. The *in situ* Raman spectra of the $x = 0.06$ sample in the temperature range of 25–190 °C are shown in Fig. 2(b). It is observed that as the temperature increased and the δ_s(VO$_4$) (B_g) and δ_{as}(VO$_4$) (A_g) modes moved closer to each other, they finally became one peak at about 105 °C. This result further confirmed that the ferroelastic phase field in the xBi(Fe$_{1/3}$Mo$_{2/3}$)O$_4$–(1−x)BiVO$_4$ ($0.0 \leq x \leq 1.0$) system is determined by composition change and high temperature. As the x value increased, the intensity of ν_s(VO$_4$) mode at 824.4 cm^{-1} became weaker and weaker. Meanwhile, the intensity of ν_s(MoO$_4$) mode at about 868 cm^{-1} increased and became the strongest peak when $x \geq 0.75$ due to the increase of Mo content in the composition. For the pure Bi(Fe$_{1/3}$Mo$_{2/3}$)O$_4$ materials, more Raman modes can be observed, as seen in Fig. 2(a), due to the ordering of Fe and Mo on the B site. The fundamental frequencies for isolated MoO$_4$ groups are $\nu_1 = 894$ cm^{-1}, $\nu_2 = 407$ cm^{-1}, $\nu_3 = 833$ cm^{-1}, and $\nu_4 = 318$ cm^{-1}, according to Weinstoc *et al.* study.[16] It can be concluded that the mode at 868 cm^{-1} was assigned to the ν_s(MoO$_4$) mode, while the modes at 315 cm^{-1} and 348 cm^{-1} could be assigned to the δ_s(MoO$_4$) mode and δ_{as}(MoO$_4$) mode, respectively, which is very similar to (Na$_{0.5}$Bi$_{0.5}$)MoO$_4$ materials.[12] The characteristic vibrations of isolated FeO$_4$ groups are $\nu_1 = 832$ cm^{-1}, $\nu_2 = 340$ cm^{-1}, $\nu_3 = 790$ cm^{-1}, and $\nu_4 = 322$ cm^{-1}.[17] The modes observed here at 776 cm^{-1} and 710 cm^{-1} can be assigned to δ_s(FeO$_4$) mode and δ_{as}(FeO$_4$) mode, respectively. The modes below 200 cm^{-1} should be assigned to the external modes (rotation/translation).

Microstructure, microwave dielectric properties, ferroelastic phase transition and their relations

SEM micrographs of as-fired surfaces demonstrate the microstructure of the xBi(Fe$_{1/3}$Mo$_{2/3}$)O$_4$–(1−x)BiVO$_4$ ceramics

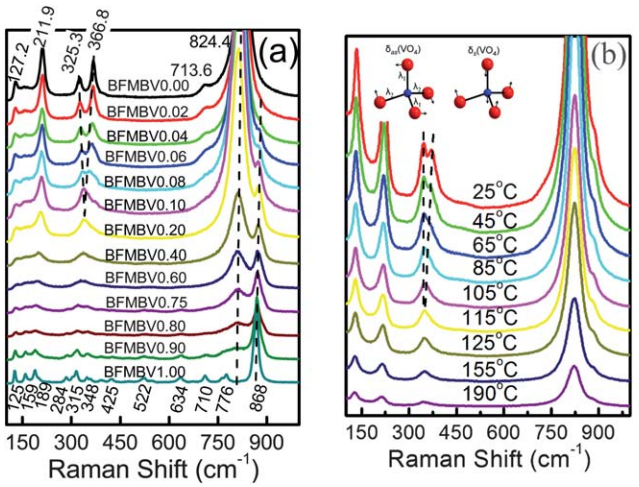

Fig. 2 Room temperature Raman spectra of xBi(Fe$_{1/3}$Mo$_{2/3}$)O$_4$–(1−x)BiVO$_4$ (0.0 ≤ x ≤ 1.0) ceramics (a) and *in situ* Raman spectra of the BFMBV0.06 sample in the temperature range 25–190 °C (b).

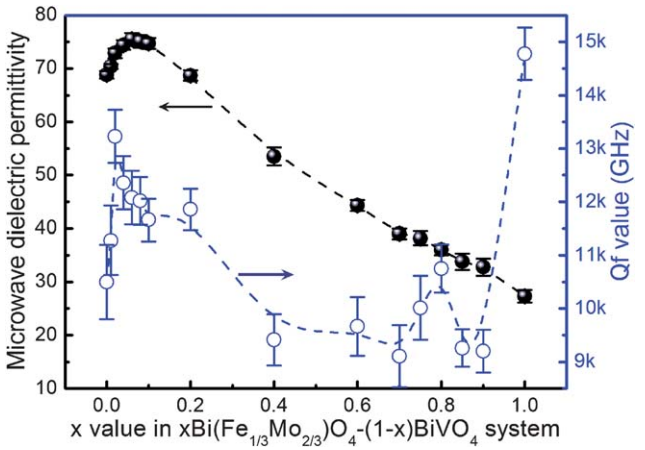

Fig. 4 Room temperature microwave dielectric properties of xBi(Fe$_{1/3}$Mo$_{2/3}$)O$_4$–(1−x)BiVO$_4$ (0.0 ≤ x ≤ 1.0) ceramics.

(x = 0.01, 0.02, 0.08, 0.20, 0.40, and 0.60) sintered at 820 °C for 2 h, as shown in Fig. 3. Dense and homogeneous microstructures with almost no pores could be revealed in all compositions. It can be seen that the grain size increased from 3–5 μm to about 4–10 μm as the x value increased from 0.01 to 0.08. With the further increase of x value to 0.60, the grain size decreased to about 1–4 μm. Due to the similar sintering temperature of the two end members BiVO$_4$ and Bi(Fe$_{1/3}$Mo$_{2/3}$)O$_4$ ceramics, there is no remarkable change of the sintering temperature in the xBi(Fe$_{1/3}$Mo$_{2/3}$)O$_4$–(1−x)BiVO$_4$ (0.0 ≤ x ≤ 1.0) ceramics, and all the ceramic samples can be densified in a narrow temperature range of 800–840 °C.

Fig. 4 shows the room temperature microwave dielectric properties of xBi(Fe$_{1/3}$Mo$_{2/3}$)O$_4$–(1−x)BiVO$_4$ (0.0 ≤ x ≤ 1.0) ceramics as a function of x value (at 4–7 GHz). The microwave permittivity first increased linearly from 69 to a maximum value of ~75.5 as the x value increased from 0.0 to 0.06, and then decreased down to 27.3 for the end member Bi(Fe$_{1/3}$Mo$_{2/3}$)O$_4$. It is a little different from the result in (A$_{0.5x}$Bi$_{1-0.5x}$)(Mo$_x$V$_{1-x}$)O$_4$ (A = Li, Na and K) systems, in which the maximum permittivity values around 80 were reached at the phase boundary of monoclinic and tetragonal phases. It might be attributed more to the larger ionic radius (0.49 Å) and the smaller polarizability (2.29 Å^3) of Fe^{3+} than that of Mo^{6+} (0.41 Å and 3.28 Å^3, respectively).[18,19] The Qf values increased approximately linearly from 10 500 GHz at x = 0.0 (4.8 GHz) to 13 200 GHz at x = 0.02 (4.8 GHz) and then decreased slowly to 10 000 GHz at x = 0.70. When the x value is increased further, the Qf value increased and reached a maximum of 14 700 GHz for the end member Bi(Fe$_{1/3}$Mo$_{2/3}$)O$_4$ (6.8 GHz). Generally, the Qf values of the ceramic compositions xBi(Fe$_{1/3}$Mo$_{2/3}$)O$_4$–(1−x)BiVO$_4$ (0.0 ≤ x ≤ 1.0) are much higher than that of the (A$_{0.5x}$Bi$_{1-0.5x}$)(Mo$_x$V$_{1-x}$)O$_4$ (A = Li, Na and K) systems (between 3000 and 10 000 GHz).[11–14]

To further understand the temperature dependence of the microwave dielectric properties, the microwave permittivity and Qf values of xBi(Fe$_{1/3}$Mo$_{2/3}$)O$_4$–(1−x)BiVO$_4$ (0.0 ≤ x ≤ 1.0) ceramics as a function of temperature (−240 to +150 °C) are presented in Fig. 5. According to the classical Lyddane–Sachs–Teller (LST) relation,[20] a maximum value of relative permittivity is expected at the phase transition temperature if there is a

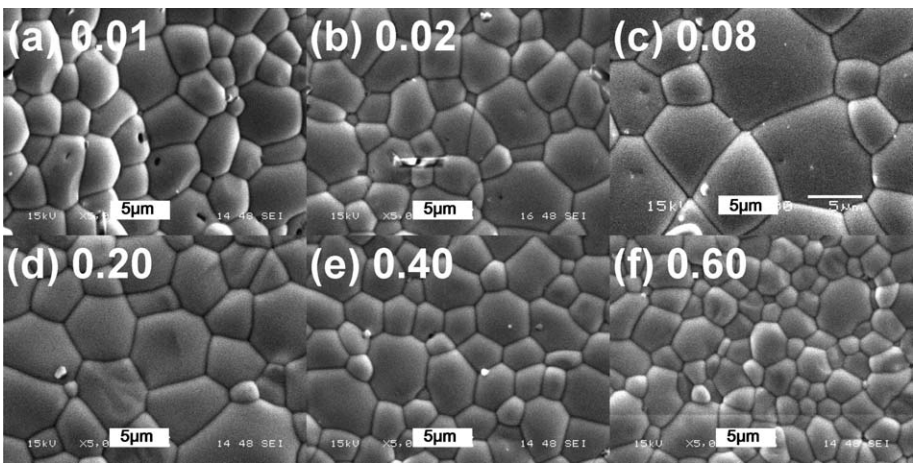

Fig. 3 SEM photos for the BFMBV0.01 ceramic (a), BFMBV0.02 ceramic (b), BFMBV0.08 ceramic (c), BFMBV0.20 ceramic (d), BFMBV0.40 ceramic (e), and BFMBV0.60 ceramic (f) sintered at 820°C per 2 h.

coupling to an optic mode, as is the case here. For example, there is a maximum permittivity value of about 77.2 observed at around 115 °C for $x = 0.06$ sample, and this corresponds well with the phase transition temperature deduced from the *in situ* Raman spectra analysis discussed above. Similarly the phase transition temperatures for $x = 0.08$ and $x = 0.10$ samples can also be obtained from the permittivity–temperature spectra to be about 61 °C and −9 °C, respectively, as seen in Fig. 5(a). However, there is no permittivity anomaly observed for $x = 0.20$ sample in the wide temperature range of −240 to +120 °C, which indicates that the tetragonal phase of this composition is stable, and the monoclinic phase cannot be induced by a displacive phase transition. For samples with $x \leq 0.04$, the ferroelastic phase transition temperatures are higher than the limit of +150 °C of our measurement system. The Qf values seem to decrease linearly with the temperature no matter whether it is the monoclinic phase or the tetragonal phase (only data for $x = 0.02$, 0.08 and 0.20 samples are presented to be clear). Although high dielectric permittivity and Qf values can be obtained in samples with $0.01 \leq x \leq 0.10$, the temperature dependence of resonant frequency or permittivity is seriously influenced by the phase transition. To obtain a temperature stable microwave dielectric ceramic, a composite sample was designed by mixing and co-firing the $x = 0.02$ sample with negative TCF and $x = 0.10$ sample with positive TCF in the temperature range 20–140 °C. The results are presented in Fig. 5, and it can be seen that quite flat spectra of permittivity about 74.8 can be obtained with high Qf values above 11 500 GHz in the composite sample (the mole ratio of BFMBV0.10 to BFMBV0.02 is around 6 to 4) sintered at 820 °C for 2 h. The biggest deviation of permittivity is about −40 ppm per °C in the wide temperature range of 20–140 °C, which means that the TCF value is about +20 ppm per °C.

Several classical microwave dielectric ceramics with permittivities larger than 70 were listed in Table 1. To the best of our knowledge, it is still very difficult to obtain a dense dielectric material with a sintering temperature below 900 °C, a permittivity ≥ 70, a Qf ≥ 5000 GHz, a TCF ≈ 0 ppm per °C, and chemical compatibility with an electrode material. The well-known $BaO–Ln_2O_3–TiO_2$ (Ln is a lanthanide) system possesses high performance of microwave dielectric properties, but its sintering temperature can not be lowered to below 1100 °C without serious deterioration of properties.[21–23] The (Ba,Sr,Ca)TiO_3 system has large permittivity between 150 and 500 and high Qf values, but it also has high sintering temperature and large positive TCF values.[24–26] It is known that the pure TiO_2 possesses large permittivity of about 104 and high Qf value above 20 000 GHz, but larger TCF value of about +465 ppm per °C and high sintering temperature around 1400 °C. Addition of CuO/zinc borosilicate glass can effectively lower its sintering temperature to around 900 °C, and the addition of $Bi_2Ti_4O_{11}$ can shift its TCF to near zero.[27–29] However, the Qf value was deteriorated (to about 3500 GHz) when both the sintering temperature and TCF values were modified.[29] Compared with the traditional microwave dielectric materials with high permittivity, the $xBi(Fe_{1/3}Mo_{2/3})O_4–(1-x)BiVO_4$ ceramics here and the $(A_{0.5x}Bi_{1-0.5x})(Mo_xV_{1-x})O_4$ (A = Li, Na and K) ceramics in our

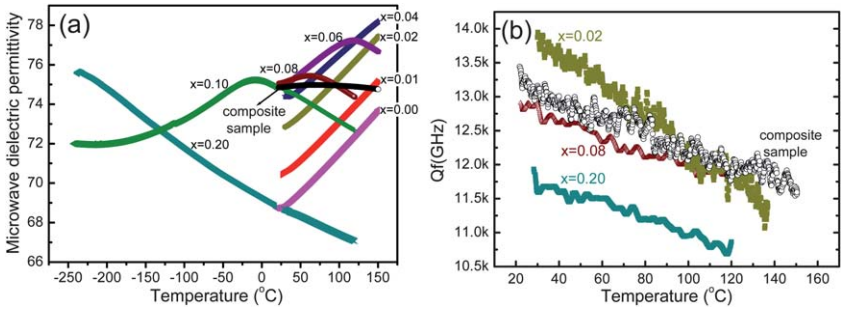

Fig. 5 Microwave dielectric permittivity (a) and Qf values (b) of $xBi(Fe_{1/3}Mo_{2/3})O_4–(1-x)BiVO_4$ ceramics as a function of temperature.

Table 1 Sintering temperatures and microwave dielectric properties of several classic microwave ceramics with permittivities larger than 70[a]

Composition	S. T. (°C)	Permittivity	Qf (GHz)	TCF (ppm per °C)	Ref.
$xBi(Fe_{1/3}Mo_{2/3})O_4–(1-x)BiVO_4$, $x = 0.02$	820	72.9 ± 0.2	13 500 ± 300	−270	This work
TiO_2 + zinc borosilicate glass	900	74	8000	340	27
$0.88TiO_2–0.012Bi_2Ti_4O_{11}$	1200	74	9500	3	28
$Ba_{2-x}Sm_{4+2/3x}Ti_9O_{24}$ ($x = 0.2$)	1370	74.8	10 900	2.4	21
$xBi(Fe_{1/3}Mo_{2/3})O_4–(1-x)BiVO_4$ $x = 0.10$	820	74.8 ± 0.2	11 600 ± 300	+170	This work
$xBi(Fe_{1/3}Mo_{2/3})O_4–(1-x)BiVO_4$ $x = 0.02$ and $x = 0.10$ composite	820	74.8 ± 0.2	13 000 ± 300	+20	This work
$(Na_{0.5x}Bi_{1-0.5x})(Mo_xV_{1-x})O_4$ $x = 0.05$ and $x = 0.10$ composite	720	77.3	10 000	<±20	12
$Ba_4Sm_{9.33}Ti_{18}O_{54}$ + 0.5 wt% B_2O_3	1200	76.1	10 500	−19	23
$0.92TiO_2–0.08Bi_2Ti_4O_{11}$ with 2 wt% CuO	900	81	3500	−5.1	29
$(Li_{0.5x}Bi_{1-0.5x})(Mo_xV_{1-x})O_4$ $x = 0.098$	650	81	8000	−90 to +9.7	11,14

[a] S. T. = Sintering Temperature.

previous work[11–14] have remarkable dielectric characteristics coupled with intrinsically low sintering temperatures. Furthermore, the Qf values have been increased substantially in xBi($Fe_{1/3}Mo_{2/3}$)O_4–(1−x)$BiVO_4$ ceramics here relative to the ($A_{0.5x}Bi_{1-0.5x}$)(Mo_xV_{1-x})O_4 (A = Li, Na and K) ceramics.

To obtain the exact phase transition temperature for samples with $x \leq 0.04$, both the DSC and thermal expansion experiments were performed. However, there is no remarkable exothermic or endothermic phenomenon observed during the phase transition, and the results are not presented here. This result implies that the ferroelastic phase transition here is a second order one without latent heat. The abnormality of the thermal expansion can be observed, and this can be used to obtain the phase transition temperature. This is a continuous change consistent with a second order transition. As shown in Fig. 6, the thermal expansion suddenly increased faster with the temperature above the phase transition temperature, which means that the coefficient of thermal expansion of the tetragonal phase is bigger than that of the monoclinic phase, which is similar to the cell parameter results for pure $BiVO_4$.[30] The phase transition temperatures of the samples with $x \leq 0.04$ can be derived from the thermal expansion data, as seen in Fig. 6. For pure $BiVO_4$, it is about 255 °C and corresponds well with the reported value.[30]

All the phase transition temperatures are plotted as a function of x value and presented in Fig. 7. It is seen that as the x value increases to 0.10, the phase transition temperature almost linearly decreases to approximately −9 °C. Earlier, Hazen and Mariathasan[30] showed a linear relationship between transition temperature and pressure as follows:

$$T\,(\mathrm{K}) = 250(\pm 3) - 15.0(\pm 3) \times P\,(\mathrm{kbar}) \quad (2)$$

A linear relationship between transition temperature and x value can also be obtained as follows in the range of $x \leq 0.10$:

$$T\,(\mathrm{K}) = 258(\pm 5) - 2550(\pm 50) \times x \quad (3)$$

These two relationships give the phase stability of $BiVO_4$, as related to the monoclinic phase under different variables, namely

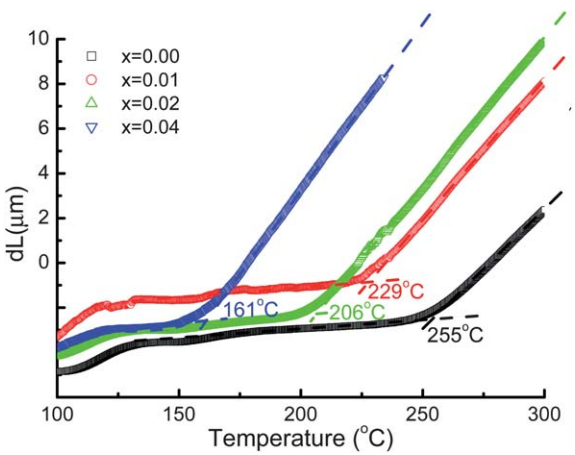

Fig. 6 Thermal expansion data of xBi($Fe_{1/3}Mo_{2/3}$)O_4–(1−x)$BiVO_4$ ceramics (x = 0.0, 0.01, 0.02, and 0.04) as a function of temperature.

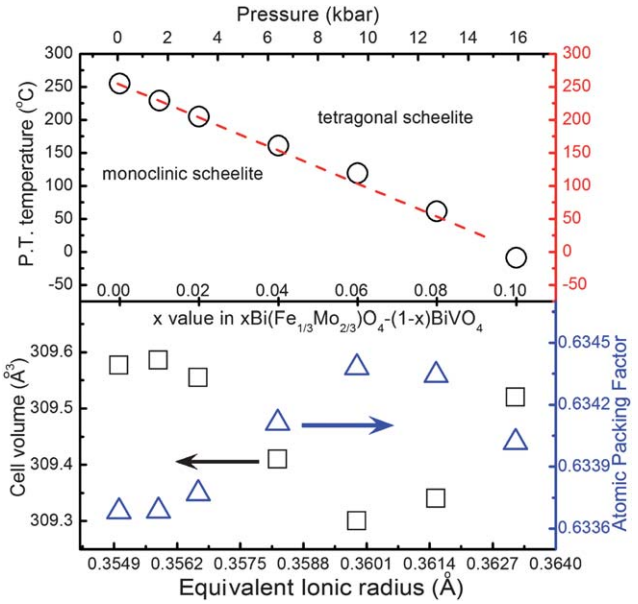

Fig. 7 Ferroelastic phase transition (monoclinic to tetragonal structure) temperature of xBi($Fe_{1/3}Mo_{2/3}$)O_4–(1−x)$BiVO_4$ ceramics ($0.0 \leq x \leq 0.10$) as a function of x value and pressure (data from ref. 30).

pressure and composition. These two relationships also help to understand the phase transition. The equivalent radius of B site ions $(Fe_{x/3}Mo_{2x/3}V_{1-x})^{5+}$ increases with the x value linearly, as shown in Fig. 7. However, the cell volume decreased slightly with the x value and reached a minimum value at $x = 0.06$, which also accounts for the maximum permittivity value discussed above. The unusual change in cell volume results in the increase of atomic packing factor in the monoclinic phase region and gives rise to the internal pressure. Hence, it is understandable that the increasing internal pressure has the similar influence on external pressure and drives the crystal structure change from the monoclinic to the tetragonal structure, which is consistent with the phase transitions.

Infrared spectra study

Fig. 8(a) presents the room temperature IR reflectivity spectra of xBi($Fe_{1/3}Mo_{2/3}$)O_4–(1−x)$BiVO_4$ ($0.0 \leq x \leq 1.0$) ceramics. It is seen that the two bands at 313 cm^{-1} and 355 cm^{-1}, which are assigned to $\delta_{as}(VO_4)$ mode and the $\delta_s(VO_4)$ mode, respectively, moved closer to each other with the increase of x value and finally merged into one band at around $x = 0.10$. This is similar to the Raman analysis above and supports the compositional phase transition at room temperature. Furthermore, the bands below 200 cm^{-1} (at least three) for pure $BiVO_4$ broadened and gradually overlapped with the increase of x value, and then could not be deconvoluted from each other at $x = 0.10$. These phenomena reflect the increase of the degree of symmetry. The *in situ* IR reflectivity spectra of the $x = 0.10$ sample are presented in Fig. 8(b). The characteristic bands splitting at 331 cm^{-1} can also be observed at around 278 K. The bands for $\delta_{as}(VO_4)$ mode and the $\delta_s(VO_4)$ mode were observed at 321 cm^{-1} and 350 cm^{-1}, respectively, at 90 K.

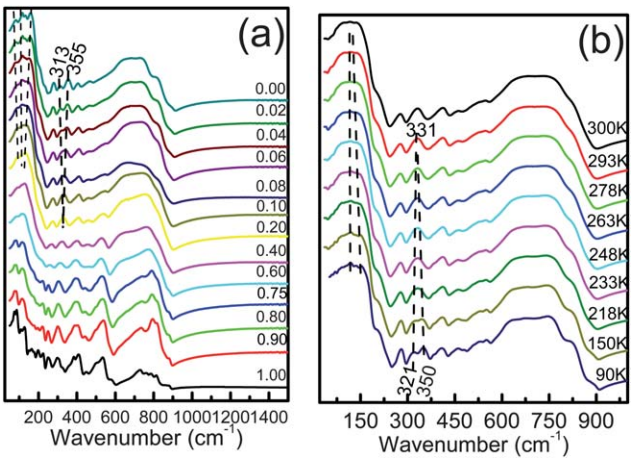

Fig. 8 Room temperature infrared reflectivity spectra of the xBi($Fe_{1/3}Mo_{2/3}$)O_4–(1−x)$BiVO_4$ (0.0 ≤ x ≤ 1.0) ceramics (a) and *in situ* high temperature Raman spectroscopy for the sample x = 0.10 (b).

The IR reflectivity spectra of Bi($Fe_{1/3}Mo_{2/3}$)O_4 were analyzed using a classical harmonic oscillator model as follows:

$$\varepsilon^*(\omega) = \varepsilon_\infty + \sum_{j=1}^{n} \frac{\omega_{pj}^2}{\omega_{oj}^2 - \omega^2 - j\gamma_j\omega} \quad (4)$$

where $\varepsilon^*(\omega)$ is a complex dielectric function; ε_∞ is the dielectric constant caused by the electronic polarization at high frequencies; γ_j, ω_{oj} and ω_{pj} are the damping factor, the transverse frequency, and the plasma frequency of the j-th Lorentz oscillator, respectively; and n is the number of transverse phonon modes. The complex reflectivity $R(\omega)$ can be written as:

$$R(\omega) = \left| \frac{1 - \sqrt{\varepsilon^*(\omega)}}{1 + \sqrt{\varepsilon^*(\omega)}} \right|^2 \quad (5)$$

The fitted IR reflectivity values and complex permittivity of pure Bi($Fe_{1/3}Mo_{2/3}$)O_4 ceramics are shown in Fig. 9(b). The dielectric permittivity at optical frequency is 1.72, and the extrapolated value at the microwave region is 23, which is a little smaller than the measured value of 27.3. The calculated dielectric loss is almost the same with the measured value. Hence, it implies that the majority of the dielectric contribution to Bi($Fe_{1/3}Mo_{2/3}$)O_4 ceramics at the microwave region can be attributed to the absorptions of structural phonon oscillation at the infrared region and very little contributions from defect phonon scattering.

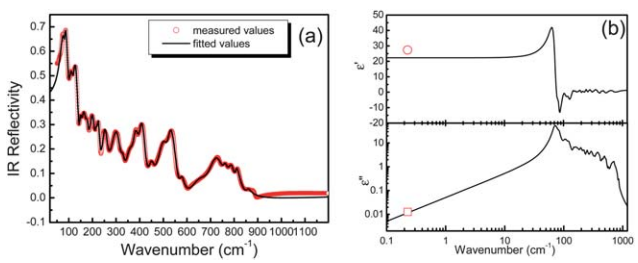

Fig. 9 Fitted IR reflectivity values (a) and complex permittivity (b) of pure Bi($Fe_{1/3}Mo_{2/3}$)O_4 ceramics.

IV. Conclusions

The xBi($Fe_{1/3}Mo_{2/3}$)O_4–(1−x)$BiVO_4$ (0.0 ≤ x ≤ 1.0) ceramics were prepared *via* the solid state reaction method and found to obtain high densities at a low sintering temperature around 820 °C. In the range 0.0 ≤ x < 0.10, a scheelite monoclinic solid solution can be formed. With the further increase of x value to 0.70, a scheelite tetragonal solid solution is stable. In the range 0.70 ≤ x < 0.90, a composite region containing scheelite tetragonal and scheelite-distorted Bi($Fe_{1/3}Mo_{2/3}$)O_4 type monoclinic phases was revealed. A Bi($Fe_{1/3}Mo_{2/3}$)O_4 type monoclinic solid solution is formed in the range 0.90 ≤ x ≤ 1.00. The ferroelastic phase transition from the scheelite monoclinic to the tetragonal structure was characterized and confirmed by *in situ* Raman and IR Reflectivity spectra, and thermal expansion data. It is suggested through an empirical pressure relationship that internal pressure within the monoclinic structure could account for the phase transition. The microwave dielectric permittivity and Qf values were proven to be dominated by the absorptions of phonon oscillation at the infrared region. A permittivity of about 74.8, a high Qf value above 11 500 GHz, and a TCF value about +20 ppm per °C can be obtained in the composite xBi($Fe_{1/3}Mo_{2/3}$)O_4–(1−x)$BiVO_4$ (0.0 ≤ x ≤ 1.0) ceramic sample, which is promising for microwave device applications.

Acknowledgements

This work was supported by the NSFC projects of China (51202182, 51202178), Fundamental Research Funds for the Central University and the headmaster foundation of Xi'an Technological University (XAGDXJJ1001). The authors would like to thank Qiu-Ping Wang, Han-Chen Liu, and Chao Zhou, for their help in Raman experiments. The authors also thank the administrators in IR beamline workstation of National Synchrotron Radiation Laboratory (NSRL) for their help in the IR measurement.

References

1 A. W. Sleight and W. J. Linn, *Ann. N. Y. Acad. Sci.*, 1976, **272**, 22.
2 M. Valant and D. Suvorov, *J. Am. Ceram. Soc.*, 2000, **83**, 2721.
3 H. Wienand, W. Ostertag and K. Bittler, *US Pat.*, 4455174, 1984.
4 J. A. Seabold and K. S. Choi, *J. Am. Chem. Soc.*, 2012, **134**, 2186.
5 A. Iwase and A. Kudo, *J. Mater. Chem.*, 2010, **20**, 7536.
6 J. Q. Yu and A. Kudo, *Adv. Funct. Mater.*, 2006, **16**, 2163.
7 A. W. Sleight and W. Jeitschko, *Mater. Res. Bull.*, 1974, **9**, 951.
8 W. Jeitschko, A. W. Sleight, W. R. McClellan and J. F. Weiher, *Acta Crystallogr., Sect. B: Struct. Crystallogr. Cryst. Chem.*, 1976, **B32**, 1163.
9 W. J. Linn and A. W. Sleight, *J. Catal.*, 1976, **41**, 134.
10 D. Zhou, L. X. Pang, J. Guo, Y. Wu, G. Q. Zhang, H. Wang and X. Yao, *J. Adv. Dielectr.*, 2011, **1**, 379.
11 D. Zhou, W. G. Qu, C. A. Randall, L. X. Pang, H. Wang, X. G. Wu, J. Guo, G. Q. Zhang, L. Shui, Q. P. Wang, H. C. Liu and X. Yao, *Acta Mater.*, 2011, **59**, 1502.
12 D. Zhou, L. X. Pang, H. Wang, J. Guo, X. Yao and C. A. Randall, *J. Mater. Chem.*, 2011, **21**, 18412.
13 D. Zhou, L. X. Pang, J. Guo, H. Wang, X. Yao and C. A. Randall, *Inorg. Chem.*, 2011, **50**, 12733.
14 D. Zhou, C. A. Randall, H. Wang, L. X. Pang and X. Yao, *J. Am. Ceram. Soc.*, 2010, **93**, 2147.
15 R. D. Shannon, *Acta Crystallogr., Sect. A: Cryst. Phys., Diffr., Theor. Gen. Crystallogr.*, 1976, **A32**, 751.

16 N. Weinstoc, H. Schulze and A. Muller, *J. Chem. Phys.*, 1973, **59**, 5063.
17 F. Gonzalez and W. P. Griffith, *J. Chem. Soc., Dalton Trans.*, 1972, **13**, 1416.
18 R. D. Shannon, *J. Appl. Phys.*, 1993, **73**, 348.
19 G. K. Choi, J. R. Kim, S. H. Yoon and K. S. Hong, *J. Eur. Ceram. Soc.*, 2007, **27**, 3063.
20 R. H. Lyddane, H. Sachs and E. Tellar, *Phys. Rev.*, 1941, **59**, 673.
21 Y. C. Chen and C. L. Huang, *Mater. Sci. Eng., A*, 2002, **334**, 250.
22 R. Ubic, I. M. Reaney and W. E. Lee, *Int. Mater. Rev.*, 1998, **43**, 205.
23 Y. Ota, K. Kakimoto, H. Ohsato and T. Okawa, *J. Eur. Ceram. Soc.*, 2003, **24**, 1755.
24 V. Subramanian, V. R. K. Murthy and B. Viswanathna, *J. Appl. Phys.*, 2001, **90**, 904.
25 H. J. Kim, S. Kucheiko, S. J. Yoon and H. J. Jung, *J. Am. Ceram. Soc.*, 1997, **80**, 1316.
26 L. Wu, Y. C. Chen, L. J. Chen, Y. P. Chou and Y. T. Tsai, *Jpn. J. Appl. Phys.*, 1999, **38**, 5612.
27 S. H. Yoon, D. W. Kim, S. Y. Cho and K. S. Hong, *J. Eur. Ceram. Soc.*, 2003, **23**, 2549.
28 A. K. Axelsson, M. T. Sebastian and M. N. Alford, *J. Korean Ceram. Soc.*, 2003, **40**, 340.
29 L. X Pang, H. Wang, D. Zhou and X. Yao, *J. Mater. Sci.: Mater. Electron.*, 2010, **21**, 1285.
30 R. M. Hazen and J. W. E. Mariathasan, *Science*, 1982, **216**, 991.